SAS Turbulence Modelling of Technical Flows

F.R. Menter and Y. Egorov

ANSYS Germany GmbH, Staudenfeldweg 12, D-83624 Otterfing, Germany
Florian.Menter@ansys.com, Yury.Egorov@ansys.com

Summary. Scale-Adaptive Simulation (SAS) allows the simulation of unsteady flows with both RANS and LES content in a single model environment. As SAS formulations use the von Karman length scale as a second external scale, they can automatically adjust to resolved features in the flow. As a result, SAS develops LES-like solutions in unsteady regions, without a resort to the local grid spacing. In the present article, a definition of the SAS modelling concept will be given. In addition, issues of the numerical treatment of the source terms will be discussed. Results will be shown for the flow in a 3D cavity and for a combustion chamber.

1 Introduction

The concept of Scale-Adaptive Simulation (SAS) [1, 2, 3, 4] allows the simulation of unsteady turbulent flows without the limitations of most Unsteady RANS (URANS) models. Contrary to standard URANS, SAS provides two independent scales to the source terms of the underlying two-equation model. In addition to the standard input in form of the velocity gradient tensor, $\partial U_i/\partial x_j$, SAS models compute a second scale from the second derivative of the velocity field. The resulting length scale is the well known von Karman length scale L_{vK}. The introduction of L_{vK} allows the model to react more dynamically to resolved scales in the flow field which cannot be handled by standard URANS models. As a result, SAS offers a single framework, which covers steady state RANS as well as LES regions, without an explicit switch in the model formulation. SAS therefore offers an attractive framework for many "multi-scale" flow problems encountered in industrial CFD.

The functionality of SAS is similar to Detached Eddy Simulation (DES) [5, 6]. It provides a steady state (or mildly unsteady) solution in stable flow regions (like boundary layers), and unsteady structures in unsteady regions within a single model framework. The difference is that the LES activity in DES is enforced by the grid limiter, whereas SAS allows a breakdown of the large unsteady structures by adapting the turbulence model to the locally

resolved length scale. In order of avoiding multiple definitions and naming conventions, as observed in DES, the following definition is given for SAS models.

1. SAS modeling is based on the use of a second mechanical scale in the source/sink terms of the underlying turbulence model. In addition to the standard input from the momentum equations in the form of first velocity gradients (strain rate tensor, vorticity tensor, ...) SAS models rely on a second scale, in the form of higher velocity gradients (second derivatives).
2. SAS models satisfy the following requirements:
   a) Provide proper RANS performance in stable flow regions.
   b) Allow the break-up of large unsteady structures into a turbulent spectrum.
   c) Provide proper damping of resolved turbulence at the high wave number end of the spectrum (resolution limit of the grid).
3. Functions 2a and 2b are achieved without an explicit grid or time step dependency in the model. Naturally, function 2c has to be based on information on the grid spacing, other information concerning the resolution limit (dynamic LES model, etc.), or the numerical method (MILES damping etc.).

In the following, two different physical formulations of the SAS model will be listed. The first is the $k - \sqrt{k}L$ model, which is the natural two-equation model environment, for which the SAS concept was developed [2]. The second formulation is for the SST model, which was augmented by Menter and Egorov [3] by the transformation of the SAS terms from the $k - \sqrt{k}L$ model. The numerical treatment of the source terms will then be discussed for the SST model. It should be noted that SAS modeling is a relatively new concept. The following formulations reflect our current best understanding of an optimal model. They are the subject of intense research and will most likely undergo some changes in the future.

2 The $k - \sqrt{k}L$ SAS Model

The details of the derivation of the model are given in [2] and are therefore not repeated here. The basic idea behind the model is to start from Rotta's $k - kL$ model [7] and to re-evaluate the critical terms, which distinguish this model from standard two-equation models. It was shown in [2] that some of the assumptions made by Rotta in the derivation of the $k - kL$ model were overly restrictive and can be relaxed. This results in the appearance of the second derivative of the velocity field in the length-scale equation, instead of the third derivative as in Rotta's model. The current version is formulated as a $k - \sqrt{k}L$ ($\Phi = \sqrt{k}L$) model:

$$\frac{\partial \rho k}{\partial t} + \nabla \cdot \rho \mathbf{U} k = P_k - c_\mu^{3/4} \rho \frac{k^2}{\Phi} + \nabla \cdot \frac{\mu_t}{\sigma_k} \nabla k \tag{1}$$

$$\frac{\partial \rho \Phi}{\partial t} + \nabla \cdot \rho \mathbf{U} \Phi = \frac{\Phi}{k} P_k \left(\zeta_1 - \hat{\zeta}_2 \kappa \frac{L}{L_{vK}} \right) - \zeta_3 \rho k + \nabla \cdot \frac{\mu_t}{\sigma_\Phi} \nabla \Phi \tag{2}$$

$$\nu_t = c_\mu^{1/4} \Phi; \quad S = \sqrt{2 \cdot S_{ij} S_{ij}}; \quad S_{ij} = \left((\nabla \mathbf{U})_{ij} + (\nabla \mathbf{U})_{ji} \right) / 2 \tag{3}$$

$$L_{vK} = \kappa \cdot S / U''; \quad U'' = \left| \nabla^2 \mathbf{U} \right| \tag{4}$$

where S is the invariant of the strain rate tensor and P_k is the production rate of the turbulent kinetic energy. The model constants are given in [2].

The SAS-relevant term in the equation for Φ is the term featuring the von Karman length scale L_{vK}. As a result of this term, the predicted turbulent length-scale L is largely proportional to the von Karman length-scale:

$$L \sim L_{vK} = \kappa \cdot S / U'' \tag{5}$$

The transformation of the $k - \sqrt{k}L$ model, with some modifications to leave the SST model undisturbed in boundary layers (model function 2a in Introduction), results in an additional term, which is simply added to the right hand side of the ω-equation of the SST model [3, 8]:

$$Q_{SST-SAS} = \rho F_{SAS} \cdot \max \left[\tilde{\zeta}_2 \kappa S^2 \frac{L}{L_{vK}} - \frac{2k}{\sigma_\Phi} \cdot \max \left(\frac{|\nabla \omega|^2}{\omega^2}, \frac{|\nabla k|^2}{k^2} \right), 0 \right] \tag{6}$$

The constants are taken from the $k - \sqrt{k}L$ model and are given in [3].

3 Discretisation in CFX Solver

The SST-SAS model has been implemented in the commercial CFD code CFX-10. Its solver is based on a finite volume formulation for structured and unstructured grids. In the case of hybrid RANS/LES or SAS simulations, the numerical switch between a second order upwind and a second order central scheme as proposed by Strelets [6] is applied for the advection terms. Switching to the non-dissipative scheme is required to let the SAS model properly resolve turbulent structures down to the grid limit (function 2b).

Satisfying the function 2c by the current implementation of the SAS model essentially depends on the way of discretising the source terms of the turbulence model. One of the main issues here is the numerical treatment of the strain rate S, which appears in the production of the turbulent kinetic energy P_k and in the SAS term $Q_{SST-SAS}$. (Calibration results for the SST-SAS model for decaying isotropic turbulence can be found in [3]). The infrastructure of the CFX solver provides different schemes for the velocity gradients, with three of them being considered for S: the standard nodal values S_N, an average of the surrounding elements $\bar{S}$ (element averaged values), and a quadratic average $\sqrt{\overline{S^2}}$.

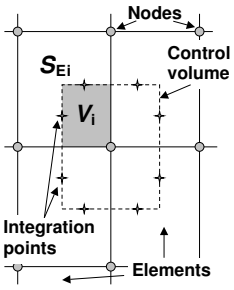

Fig. 1. Element averaged values in finite volume scheme.

The element averaging using the volume-weighting rule is shown in Figure 1:

$$\bar{S} = \frac{1}{V} \sum_{elements} V_i \, S_{Ei} \tag{7}$$

where the S_{Ei} are computed at the centers of the elements from the nodal velocities and $V = \sum V_i$. The sum is taken over all elements contributing to the control volume.

The relevant source terms in the CFX implementation are computed as:

$$P_k \sim \mu_t \overline{S^2}; \quad L_{vK} = \kappa \frac{\bar{S}}{U''}; \quad \tilde{\zeta}_2 \kappa \bar{S}^2 \frac{L}{L_{vK}} \text{ in } Q_{SST-SAS} \tag{8}$$

The above treatment of the strain rate provides function 2c (Introduction). Assuming source term equilibrium conditions, the eddy viscosity resulting from the SST-SAS model is given by [3]:

$$\mu_t = \left[\frac{1}{F_{SAS} \kappa \tilde{\zeta}_2} \left(\frac{\beta}{c_\mu} - \alpha \right) \right]^2 \cdot \rho L_{vK}^2 S \tag{9}$$

This makes clear, that the high wave number damping depends on the specific implementation of S. For a 1D velocity field $U = U(y)$ the two different discretisations S_N and $\bar{S}$ of the strain rate S give:

$$S_N = \left| \frac{U_{i+1} - U_{i-1}}{2\Delta y} \right|; \quad \bar{S} = \frac{1}{2} \left(\left| \frac{U_{i+1} - U_i}{\Delta y} \right| + \left| \frac{U_i - U_{i-1}}{\Delta y} \right| \right) \tag{10}$$

Clearly both formulations are second order in space and are nearly equivalent in a smoothly resolved flow field. However in the extreme case of the odd-even grid oscillation $U_i = \pm U_0$ one gets:

$$S_N = 0 \longrightarrow L_{vK} = 0 \quad \text{whereas} \quad \bar{S} = \frac{2U_0}{\Delta y} \longrightarrow L_{vK} = \frac{1}{2} \Delta y \tag{11}$$

The latter is a more physically correct representation of the resolved length scale (L_{vK}), which by definition cannot fall below the grid spacing (times a constant). The low values for L_{vK} resulting from the use of nodal gradients are not sufficient for providing the required damping for the smallest resolved scales.

An important next step in the development of the SAS methodology is a more generic way of providing the function 2c, including a calibration constant to adjust the method to different numerical schemes.

4 Industrial Applications

4.1 3-D Acoustic Cavity

Air flow past a 3-D rectangular shallow cavity is calculated in this test, with the cavity geometry and flow conditions corresponding to the M219 experimental test case of [9]. The geometry dimensions of the cavity are $L \times W \times D = 5 \times 1 \times 1$ (length, width, and depth), with the depth of $4''$ (all sizes in inches). The side boundaries are treated as symmetry planes, the top boundary is a far-field boundary, and all the solid surfaces are adiabatic non-slip walls. The amount of ambient space, included into the computational domain, is: $31''$ from the inlet to the cavity leading edge, $21''$ from the cavity trailing edge to the outlet, $68''$ from the cavity opening level to the top boundary. Space equal to a half of the cavity width is left between each of the side boundaries and the correspondent side edge of the cavity. The inlet Mach number is 0.85. The grid consists of $1.05 \cdot 10^6$ hexahedral elements. The time step for the simulation is $2 \cdot 10^{-5}$ s, which is 18 times less than the hydrodynamic time scale based on the inlet velocity and the cavity depth. 10^4 time steps have been computed.

Figure 2 shows the turbulent structures, produced by the SST-SAS model. Figure 3 shows the power spectral density of the transient pressure signal, calculated and measured at the K29 sensor location on the cavity bottom near the downstream wall. Despite the relatively coarse grid and short calculated physical time, the main acoustic modes are predicted in good agreement with the experiment. The simulation is currently running on a finer grid.

4.2 ITS Combustion Chamber

The instabilities in gas turbine combustion chambers are of strong technical interest, as they can produce noise and also compromise the structural integrity of the chamber. The unsteadiness can be caused by different mechanisms like flow instabilities introduced by the high swirl in the burner or thermo-acoustic instabilities from combustion itself.

The SST-SAS model is applied to the ITS test rig with a single burner. This burner is typical for industrial gas turbine combustion systems. The test rig was built as a rectangular combustion chamber. This configuration was investigated experimentally by Schildmacher and Koch [10]. A lean preheated methane-air mixture is supplied through a ring inlet with the external diameter of 120 mm, which encircles an additional axial inlet of the preheated dilution air. A partially premixed combustion model [11] available in CFX is used for this simulation. The grid consists of $3.6 \cdot 10^6$ tetrahedral elements, corresponding to $6 \cdot 10^5$ control volumes of the dual mesh.

As the experimental data are only available in the central part of the chamber, the ITS combustion chamber serves mainly as a test for the LES-capabilities of the SAS approach. It should be noted however, that industrial

combustion chambers are very complex, making a complete LES simulation impractical.

The flow structures for the cold and the hot flow simulation at a given instance in time are shown in Figures 4 and 5. Experience shows that RANS models are not able to predict the change in flow topology indicated by that figure. This can be seen in more detail in Figures 6–10 showing the radial distributions of the statistically averaged velocity and temperature at the distance from the inlet, approximately equal to one ring diameter (note the the SST and the $k-\epsilon$ model are virtually identical for free shear flows). Superior accuracy of SAS results relative to the RANS simulation confirms, that SAS is a viable method for such a complex flow.

5 Acknowledgment

The current work was partially supported by the EU within the research projects DESIDER (Detached Eddy Simulation for Industrial Aerodynamics) under contract No. AST3-CT-200-502842 (http://cfd.me.umist.ac.uk/desider) and PRECCINSTA (ENK5-CT-2000-00060).

References

1. Menter F R, Kuntz M, Bender R (2003) A scale-adaptive simulation model for turbulent flow predictions. AIAA Paper 2003-0767
2. Menter F R, Egorov Y (2005) Re-visiting the turbulent scale equation. In: Heinemann H-J (ed) Proc. IUTAM Symposium "One hundred years of boundary layer research". Göttingen, Germany, 12-14 August, 2004. Kluwer Academic Publishers (in press)
3. Menter F R, Egorov Y (2005) A Scale-adaptive simulation model using two-equation models. AIAA paper 2005–1095
4. Menter F R, Egorov Y (2005) Turbulence models based on the length-scale equation. In: Humphrey J A C, Gatski T B, Eaton J K, Friedrich R, Kasagi N, Leschziner M A (eds) Proc. Fourth International Symposium on Turbulence and Shear Flow Phenomena. Williamsburg, VA USA, 27–29 June, 2005.
5. Spalart P R (2000) Strategies for turbulence modelling and simulations. Int J Heat Fluid Flow 21:252–263
6. Strelets M (2001) Detached eddy simulation of massively separated flows. AIAA paper 2001-0879
7. Rotta J C (1972) Turbulente Strömungen. Teubner Verlag, Stuttgart
8. Menter F R (1994) Two-equation eddy-viscosity turbulence models for engineering applications. AIAA Journal 32(8):269–289
9. Henshaw M J de C (2000) M219 cavity case. In: Verification and validation data for computational unsteady aerodynamics, Tech. Rep. RTO-TR-26, AC/323/(AVT)TP/19:453–472
10. Schildmacher K-U, Koch R, Wittig S, Krebs W, Hoffmann S (2000) Experimental Investigations of the Temporal Air-Fuel Mixing Fluctuations and Cold Flow Instabilities of a Premixing Gas Turbine Burner. ASME Paper 2000-GT-0084

11. Zimont V L, Biagioli F, Syed K (2001) Modelling turbulent premixed combustion in the inter-mediate steady propagation regime. Progress in Computational Fluid Dynamics 1:14–28

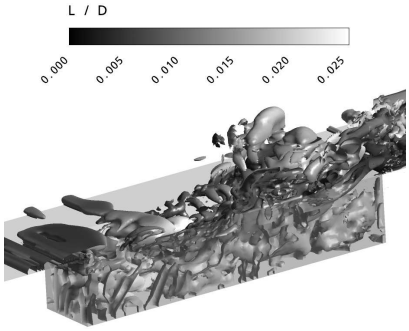

Fig. 2. 3-D acoustic cavity. Isosurface $\Omega^2 - S^2 = 10^5\ s^{-2}$, coloured by the turbulence length scale $k^{0.5}/c_\mu^{0.25}\omega$, divided by the cavity depth.

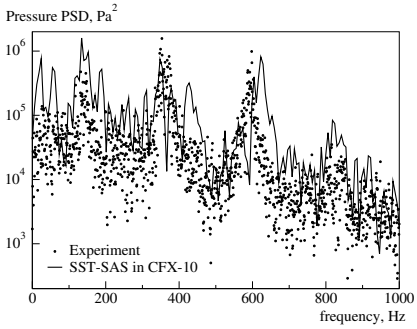

Fig. 3. 3-D acoustic cavity. Power spectral density of the pressure signal, measured by a sensor K29 on the cavity bottom close to the downstream wall.

Fig. 4. ITS combustion chamber, non-reacting. Isosurface $\Omega^2 - S^2 = 10^5\ s^{-2}$.

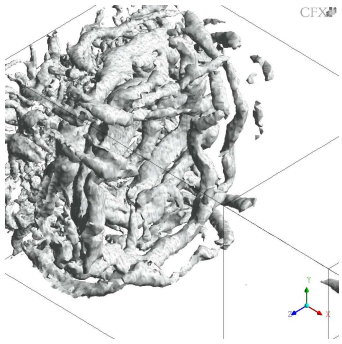

Fig. 5. ITS combustion chamber, reacting. Isosurface $\Omega^2 - S^2 = 10^5\ s^{-2}$.

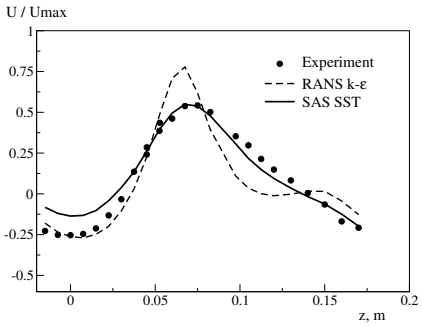

Fig. 6. Non-reacting combustion chamber. Axial velocity profile at x=138 mm.

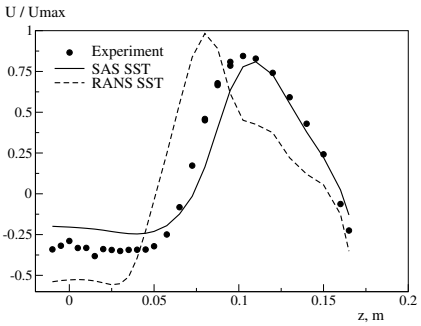

Fig. 7. Reacting combustion chamber. Axial velocity profile at x=103 mm.

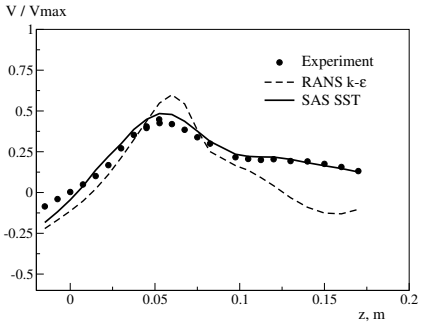

Fig. 8. Non-reacting combustion chamber. Tangential velocity at x=138 mm.

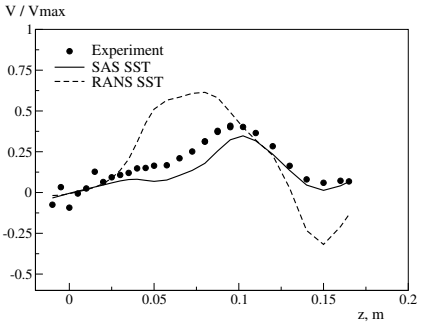

Fig. 9. Reacting combustion chamber. Tangential velocity at x=103 mm.

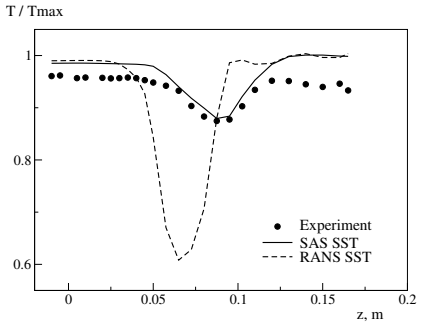

Fig. 10. Reacting combustion chamber. Temperature profile at x=103 mm.